The Meteoritical Society

Meteoritics & Planetary Science 42, Nr 11, 1945–1960 (2007)
Abstract available online at http://meteoritics.org

Impact metamorphism of $CaCO_3$-bearing sandstones at the Haughton structure, Canada

Gordon R. OSINSKI

Canadian Space Agency, 6767 Route de l'Aeroport, Saint-Hubert, Quebec, J3Y 8Y9, Canada
Present address: Department of Earth Sciences and Department of Physics and Astronomy, University of Western Ontario, 1151 Richmond Street, London, ON, N6A 5B7, Canada
E-mail: gosinski@uwo.ca

(Received 16 October 2006; revision accepted 11 July 2007)

Abstract–Impact-metamorphosed $CaCO_3$-bearing sandstones at the Haughton structure have been divided into 6 classes, based to a large extent on a previous classification developed for sandstones at Meteor Crater. Class 1a sandstones (<3 GPa) display crude shatter cones, but no other petrographic indications of shock. At pressures of 3 to 5.5 GPa (class 1b), porosity is destroyed and well-developed shatter cones occur. Class 2 rocks display planar deformation features (PDFs) and are characterized by a "jigsaw" texture produced by rotation and shear at quartz grain boundaries. Calcite shows an increase in the density of mechanical twins and undergoes micro-brecciation in class 1 and 2 sandstones. Class 3 samples display multiple sets of PDFs and widespread development of diaplectic glass, toasted quartz, and symplectic intergrowths of quartz, diaplectic glass, and coesite. Textural evidence, such as the intermingling of silicate glasses and calcite and the presence of flow textures, indicates that calcite in class 3 sandstones has undergone melting. This constrains the onset of melting of calcite in the Haughton sandstones to >10 < 20 GPa. At higher pressures, the original texture of the sandstone is lost, which is associated with major development of vesicular SiO_2 glass or lechatelierite. Class 5 rocks (>30 GPa) consist almost entirely of lechatelierite. A new class of shocked sandstones (class 6) consists of SiO_2-rich melt that recrystallized to microcrystalline quartz. Calcite within class 4 to 6 sandstones also underwent melting and is preserved as globules and euhedral crystals within SiO_2 phases, demonstrating the importance of impact melting, and not decomposition, in these $CaCO_3$-bearing sandstones.

INTRODUCTION

Hypervelocity impact events are catastrophic, near-instantaneous geological events. They generate pressures and temperatures that can vaporize, melt, metamorphose, and/or deform a substantial region of the target sequence. This results in the formation of shock metamorphic indicators, either megascopic (e.g., shatter cones) or microscopic (e.g., planar deformation features ([PDFs]), and high-pressure polymorphs (e.g., coesite and stishovite from quartz). Impact metamorphism is essentially the same as shock metamorphism except that it also encompasses the melting and vaporization of target rocks and post-impact processes, such as post-shock cooling and contact metamorphism (Stöffler and Grieve 1994). The recognition of shock metamorphism in the 1960s was a critical advancement in the field of impact geology as it provided an important tool for the recognition of meteorite impact structures (see papers in French and Short 1968).

Current classifications of shock metamorphic stages are based almost entirely on features developed in dense, nonporous crystalline rocks (Stöffler 1971; Kieffer et al. 1976a; Grieve et al. 1996). Sedimentary rocks are present in the target sequence of ~70% of the world's known impact structures (Earth Impact Database 2007); however, the only available shock classification for such lithologies is one for sandstones based on the pioneering studies of S. Kieffer and co-workers at Meteor Crater, Arizona (Kieffer 1971; Kieffer et al. 1976b). These studies demonstrated the dramatic effects of porosity, grain characteristics, volatiles, and layering, on the response of quartz to impact in sedimentary targets. For example, Kieffer et al. (1976b) showed that in Coconino Sandstone from Meteor Crater, diaplectic glass forms in rocks at pressures as low as ~5.5 GPa, with the generation of vesicular SiO_2 glass at ~20 GPa and whole rock melting occurring above ~30 to 35 GPa (Fig. 1). For quartz in non-porous crystalline rocks, diaplectic glass is observed in the pressure range from 32.5 to

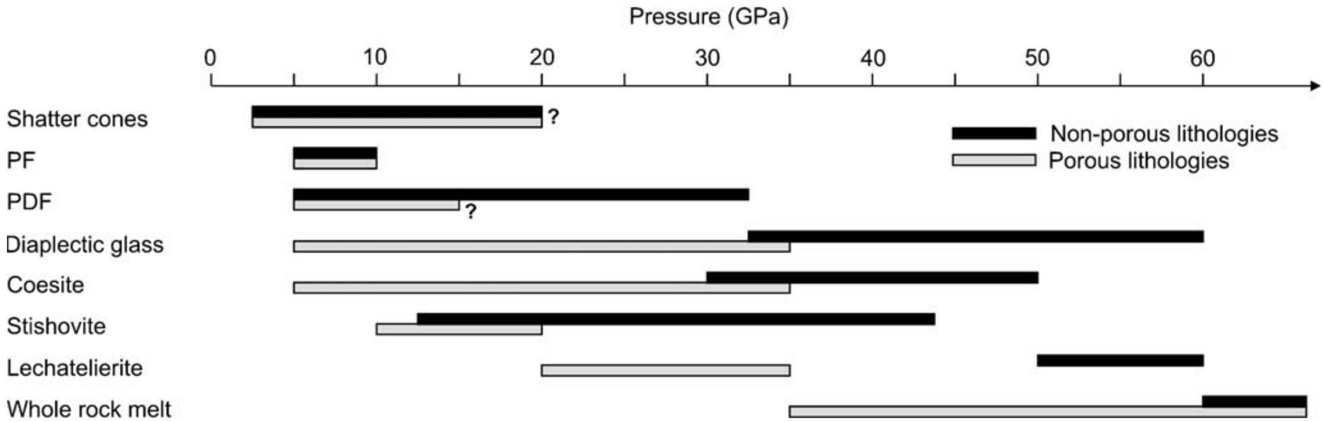

Fig. 1. Summary and comparison of the important shock metamorphic effects developed in quartz in porous and non-porous targets. Compiled with data from Kieffer et al. (1976) and Grieve et al. (1996).

50 GPa, with whole rock melting commencing over the range ~50 to 60 GPa (Grieve et al. 1996) (Fig. 1).

The recognition and classification of shock metamorphic stages in carbonates, on the other hand, is a difficult and unresolved problem. Early workers recognized the common occurrence of shatter cones in limestone (Robertson and Mason 1975) and the intense twinning of calcite (Robertson and Grieve 1978) at the Haughton impact structure, which they ascribed to the impact event. Subsequently, lattice defects (fractures and planar defects) that "could be interpreted as direct shock effects" were recognized in carbonates, also at Haughton (Martinez et al. 1994a). Shock experiments and thermodynamic calculations can provide important information regarding shock processes; however, for carbonates, such techniques currently provide contrasting and ambiguous results regarding the response of carbonates to hypervelocity impact (Table 1). For example, early experimental studies suggested that calcite undergoes significant decomposition (>10–50%) at pressures as low as 10 to 20 GPa (e.g., Lange and Ahrens 1986). More recently, Skála et al. (2002) presented results, which suggest that decomposition of calcite only occurs at pressures >65 GPa. The complete shock melting of $CaCO_3$ at pressures of ~25 GPa and temperatures of ~2700 K was also recently demonstrated in shock experiments (Langenhorst et al. 2000).

Attempts have also been made to quantify shock effects in carbonates using X-ray diffraction (XRD) and electron spin resonance (ESR) (Polanskey and Ahrens 1994; Skála and Jakeš 1999; Skála et al. 1999; Skála et al. 2002; Burt et al. 2005); however, calibration of the observed effects with respect to shock pressure remains ambiguous so that these methods remain qualitative at present. Recently, the first detailed application of twin analysis in calcite has been used to quantify shock pressures in carbonates from Serpent Mound, USA (Schedl 2006). Given that low shear stresses of ~10 MPa are required for twinning in calcite (Schedl 2006), this technique may prove a useful shock indicator for carbonates at relatively low shock levels. At higher pressures (i.e., within the realm of impact metamorphism), studies of naturally shocked rocks (see Osinski et al. 2008 for a review) combined with the reappraised phase relations of $CaCO_3$ (Ivanov and Deutsch 2002), suggest that the dominant response of carbonates to hypervelocity impact is melting.

In this contribution, a series of variably shocked calcite-bearing sandstones from the Haughton impact structure have been studied. This represents the first detailed study of such lithologies at Haughton and builds upon preliminary work presented by (Osinski 2005), and earlier work on shocked sandstones from this site (Metzler et al. 1988; Redeker and Stöffler 1988; Osinski et al. 2005a). By comparing the shock effects in calcite with known, calibrated effects in quartz, a better understanding of the response of calcite to hypervelocity impact has been made possible.

GEOLOGICAL SETTING OF THE HAUGHTON IMPACT STRUCTURE

The Haughton impact structure is a well preserved ~39 Ma complex impact structure situated on Devon Island in the Canadian High Arctic (75°22′N, 89°41′W) (Figs. 2a, 2b) (Grieve 1988; Osinski et al. 2005b). Detailed structural mapping indicates that Haughton has an apparent crater diameter of 23 km and a rim (final crater) diameter of ~16 km (Osinski and Spray 2005). The target rocks comprise an almost flat-lying unmetamorphosed ~1880 m thick sequence of Lower Paleozoic sedimentary rocks of the Arctic Platform, overlying Precambrian metamorphic basement of the Canadian Shield (Figs. 1b, 1c) (Thorsteinsson and Mayr 1987). The sedimentary sequence is dominated by carbonates, with minor evaporates, shales, and sandstones (Fig. 2c). Sandstones are most common in the lowermost Ordovician and Cambrian successions (Fig. 2c).

Haughton possesses a complex central uplift comprising three contrasting structural zones (Osinski and Spray 2005). A central ~2 km diameter core of differentially uplifted megablocks, is surrounded by a zone of kilometer-size fault-bounded blocks displaying more moderate dips (~10–40°) (Fig. 2b). The

Table 1. Compilation of experimental and modeling data on the shock behavior of carbonates. Table modified and updated from Agrinier et al. (2001) and Osinski et al. (2008).[1]

Pressure (GPa)	Material	Experimental method(s)	Observed effect(s)	Reference
10–42	Cc, single crystal	Shock reverberation; sample recovery	10 to 67% devolatilization, non-homogeneous	Lange and Ahrens (1986)
10	Chalk, 49% porosity	Impedance matching; particle velocity measurements	90% devolatilization	Tyburczy and Ahrens (1986)
17	Aragonite, single crystal, 1.7% porosity	Impedance matching; particle velocity measurements	Onset of devolatilization	Vizgirda and Ahrens (1982)
18	Cc, single crystal	Impedance matching; trapping of gas	Onset (~0.3 mol%)	Boslough et al. (1982)
20	Cc, single crystal	Shock reverberation; sample recovery	~50% devolatilization	Lange and Ahrens (1986)
25	Lst., polycrystalline	Impedance matching; particle velocity measurements	20–30% devolatilization	Tyburczy and Ahrens (1986)
25	Cc, single crystal	Multi-anvil; fast decompression	Mechanical twins and dislocations	Langenhorst et al. (2000, 2002)
25	Cc, compacted powder	Multi-anvil; fast decompression	Melting; formation of fine-grained foamy Cc aggregate	Langenhorst et al. (2000, 2002)
30	Lst., polycrystalline	Impedance matching; single shocks; sample recovery	13% devolatilization	Kotra et al. (1983)
>30	Dol. rock, polycrystalline	Impedance matching; sample recovery	Possible formation of periclase	Skála et al. (1999)
33	Cc, non-porous	Calculation of post-shock entropy; isentropic release	Onset of devolatilization	Vizgirda and Ahrens (1982)
35–45	Cc	Shock reverberation; sample recovery	Onset to complete devolatilization	Martinez et al. (1995)
40	Cc, single crystal	Impedance matching color T measurements	High T shear band regions with T 5 2200 K	Kondo and Ahrens (1983)
40–50	Cc, Arag., non-porous	Calculations	Onset of devolatilization	Pasternak et al. (1976)[2]
45	Cc	Calculation of post-shock energy Hugoniot	Onset of devolatilization	Kieffer and Simonds (1980)
55	Arag., non-porous	Calculation of post-shock entropy; isentropic release	Onset of devolatilization	Vizgirda and Ahrens (1982)
55–65	Dol.	Shock reverberation; sample recovery	Onset to complete devolatilization	Martinez et al. (1995)
<60	Lst., dol, solid disks	Shock reverberation; sample recovery	Stable	Bell et al. (1998b)
<60	Cc, single crystal	Impedance matching; sample recovery	Minor, if any devolatilization	Kotra et al. (1983)
<60	Dol. rock, polycryst. 4–6% porosity	Shock reverberation; sample recovery	Decrease in grain size	Martinez et al. (1995)
60	Cc, single crystal	Shock reverberation; thermal gravimetric analysis	7% CO_2 loss	Bell (2001)
60	Dol. rock, polycryst. 4–6% porosity	Shock reverberation; pre-heating; sample recovery	nm-sized periclase crystals	Martinez et al. (1994b)
>60 <68	Dol. rock, polycryst.	Impedance matching; sample recovery	Relatively stable; <1 µm size periclase crystals	Skála et al. (2002)
61	Cc	Shock reverberation; sample recovery	Recrystallized Cc; probably from a melt	Badjukov et al. (1995)
64 < 85	Cc, single crystal	Shock reverberation; sample recovery	Mechanical twins and dislocations	Ivanov et al. (2002)
64 < 85	Cc, compacted powder	Shock reverberation; sample recovery	Melting; formation of fine-grained foamy Cc aggregate	Ivanov et al. (2002)
70	Cc	Hydrocode modeling of shock experiments	No decomposition	Ivanov et al. (2002)
85	Cc, single crystal	Shock reverberation; sample recovery	Mechanical twins and dislocations	Langenhorst et al. (2002)
85	Cc, compacted powder	Shock reverberation; sample recovery	Melting; formation of fine-grained foamy Cc aggregate	Langenhorst et al. (2002)
>70	Dol. rock, polycryst.	Impedance matching; sample recovery	Disintegration of sample containers apparently due to extensive vapor production	Skála et al. (2002)
224	Cc	Laser irradiation	Relatively stable; crack development	Langenhorst et al. (2002)

[1]The wide variation in results is likely due to several factors including differences between experimental techniques (single shock versus reverberation), and/or properties of the sample material (e.g., porosity), and/or the duration of the shock state (see Langenhorst et al. 2002 and Osinski et al. 2008 for reviews and discussion). Abbreviations: Cc = calcite; Lst. = limestone; Dol. = dolomite; Arag. = aragonite; polycryst = polycrystalline.

[2]Unpublished work cited in Boslough et al. (1983).

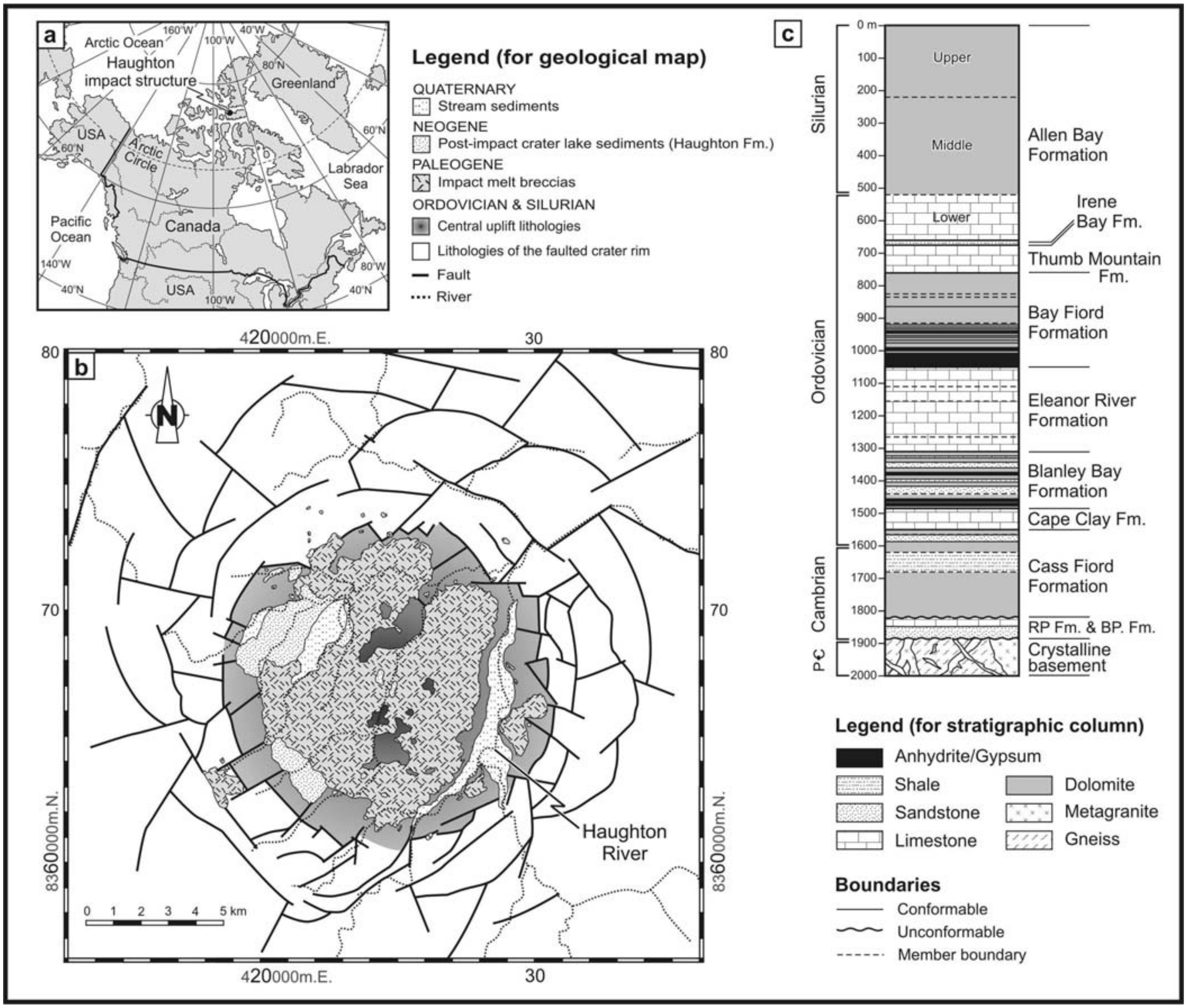

Fig. 2. a) Location of the Haughton impact structure in the Canadian High Arctic. b) Simplified geological map of the Haughton structure. c) Stratigraphic column showing the target sequence at the Haughton structure at the time of impact. Compiled with data from Thorsteinsson and Mayr (1987) and modified from Osinski et al. (2005b). Abbreviations: Fm. = Formation; RP = Rabbit Point; BP = Bear Point.

outermost zone of the central uplift extends out to a radial distance of ~5.0 to 6.5 km and consists of a structural ring of intensely faulted (sub-) vertical and/or overturned strata. The central uplift is surrounded and overlain by a series of parautochthonous and allochthonous impact breccias (Redeker and Stöffler 1988; Osinski et al. 2005a). Carbonate-rich impact melt breccias are volumetrically the most important impactite lithology, forming a virtually continuous ~54 km^2 layer covering the central area of the Haughton structure (Fig. 2b), with a maximum current thickness of ~125 m, and a present volume of ~7 km^3. These pale gray weathering impactites contain variably shocked clasts from depths of ~700–2000 m in the pre-impact target sequence, enclosed in a melt groundmass of calcite, silicate impact melt glass, and anhydrite (Osinski and Spray 2001, 2003; Osinski et al. 2005a).

SAMPLES AND ANALYTICAL TECHNIQUES

Approximately 110 individual centimeter- to decimeter-size clasts of impact-metamorphosed sandstones were collected from throughout the crater-fill impact melt breccias over the course of 8 field expeditions to the Haughton structure. Eight samples of sandstone from two megablocks from the inner part of the central uplift were also collected. Polished thin sections were prepared from 60 samples. Following petrographic observations, 17 samples, primarily shock-melted lithologies in which the protolith was uncertain (e.g., a possible chert or quartz-bearing carbonate origin could not be ruled out), were excluded from further study (see Appendix for sampling locations of the 43 samples investigated in detail as part of this work). A JEOL JXA-8900 L electron microprobe equipped with a wavelength dispersive X-ray (WDS) spectrometer was used to obtain quantitative chemical analyses and element maps using beam operating conditions of 15 kV and 20 nA. Back-scattered electron (BSE) imagery was used to investigate the micro-textures of the various samples. X-ray diffraction (XRD) was performed on bulk pressed powdered samples using a Phillips PW 1050 diffractometer equipped with a Cu X-ray source and operated at 40 kV and 30 mA. X-ray microdiffraction was carried out on select samples to further investigate the distribution and characteristics of various SiO_2 and $CaCO_3$ phases. This was carried out with a 50 × 50 μm spot size on polished thin sections using a Bruker DISCOVER X-ray diffractometer at the University of Western Ontario, Canada.

This study also incorporated unpublished observations of millimeter-size clasts of shock-metamorphosed sandstones from a previous study of 90 polished thin sections of impact melt breccias, together with published data on shock-melted sandstones (Osinski et al. 2005a).

RESULTS

Impact-metamorphosed sandstones from Haughton have been divided into six classes, following the shock classification scheme developed by Kieffer (1971) and Kieffer et al. (1976b) (Table 1). The quoted pressure estimates for each class are from Kieffer (1971) and Kieffer et al. (1976b). It should be noted that class 6 has been added here to the original classification scheme of Kieffer (1971) and two classes have been subdivided.

Class 0 (<<1 GPa)

Unshocked sandstones *sensu stricto* are not exposed in the environs of the Haughton structure; however, several sandstones collected from up to ~80 km outside the crater are typically mature, fine-grained (longest dimensions <0.5–1.0 mm) quartz arenites, comprising well-rounded quartz grains. The samples are well sorted, grain-supported and comprise a cement of quartz and/or calcite (sparite). Rare grains of calcite (<5 vol%) and variable amounts of K-feldspar (up to ~10 vol%) are also present. Typical porosity values range from ~5 to 25 vol%.

Sandstones with no recognizable signs of shock are found within parautochthonous and allochthonous impact breccias in the crater interior. These lithologies have been affected by the passage of the shock wave and are, therefore, not considered to be completely unshocked, but they can provide information regarding the properties of sandstone target rocks. Importantly, the petrography of these low shock level sandstones is consistent with the unshocked sandstones collected from outside the Haughton structure.

Class 1 (<5.5 GPa)

Class 1a rocks show no recognizable signs of shock using optical and BSE imaging techniques (Table 2). Crude shatter cones are present at the outcrop and hand specimen scale. Class 1a lithologies preserve a petrographically observable remnant porosity (cf. shocked sandstones from Meteor Crater; Kieffer 1971). The presence of well-developed shatter cones in class 1b samples coincides with a gradual reduction and eventual destruction of original porosity (Table 2) (Figs. 3a–c). (It should be noted that although class 1b samples lack observable remnant porosity using optical microscopy, in BSE images, micrometer-size pore spaces are present (Table 2), although these cavities may represent defects from the thin section preparation process.) Kieffer (1971) suggests that pressures of >3 and <5.5 GPa are required to eliminate porosity during shock compression. Minor planar fractures but no planar deformation features were observed in quartz in class 1b samples (Table 2). Calcite in class 1 rocks shows a progressive decrease in grain size and an increase in the density of mechanical twins (Table 2).

Class 2 (~5.5 to 10 GPa)

Figure 4 shows a series of images of class 2 sandstones that display the classic “jigsaw” texture, first described by Kieffer (1971) in shocked sandstones from Meteor Crater. This texture is produced by rotation and shear at quartz grain boundaries, leaving the interiors of grains relatively undamaged (Kieffer et al. 1976b). In contrast to quartz, calcite in class 2 sandstones has been reduced to fine-grained polycrystalline “micro-breccias” (Fig. 4c), most likely through abrasion of misfitting grain surfaces (cf. shocked limestones from the Ries impact structure, Germany; Barber and Wenk 1973). Class 2 sandstones are also characterized by the presence of PDFs in quartz and minor development of so-called toasted quartz (Table 2) (see Whitehead et al. 2002, for a discussion of toasted quartz). X-ray microdiffraction demonstrates the presence of trace amounts of coesite in class 2 sandstones.

Class 3 (~10 to 20 GPa)

Class 3 sandstones at Meteor Crater are characterized by the preservation of original sedimentary textures (e.g., layering, sorting, etc.) associated with the presence of coesite and the development of diaplectic glass (Kieffer 1971). Class 3 sandstones from Haughton have been subdivided in this study into two subtypes based on the very high abundance of diaplectic glass in several samples (Table 2), while still preserving the original sedimentary fabric (Fig. 5a). This distinguishes class 3 from class 4 sandstones (Kieffer 1971).

Class 3a and 3b rocks show the widespread development of “symplectic regions” (Table 2) (Figs. 5b–e), which are distinguished in transmitted light by their very high relief and the presence of opaque regions (Fig. 5b). X-ray microdiffraction demonstrates that these symplectic regions represent microscopic intergrowths of quartz, coesite and diaplectic glass (Fig. 6) (cf. Kieffer 1971). This study also shows that these symplectic regions are observable in BSE

Table 2. Classification of impact metamorphic effects displayed by $CaCO_3$-bearing sandstones from the Haughton impact structure.

Class	Pressure range (GPa)[a]	Temp. range (°C)[a]	Hand specimen observations	Porosity (%)[b]	Proportion of various SiO_2 phases and effects (vol%)[c]					Microscopic observations	
					Qtz	Dg	Lech	Coesite	Toast	SiO_2 phases	Calcite[d]
1a	<3	<350	Crude shatter cones; pale yellow–brown	7–23	100 (100)	None (none)	None (none)	None (none)	None (N/A)	Recognizable porosity; no indications of shock	No indications of shock
1b	3–5.5	<350	Well developed shatter cones; pale yellow-brown	2–5	100 (100)	None (none)	None (none)	None (none)	None (N/A)	No recognizable porosity using optical microscopy; fracturing of quartz grains; minor development of PFs	Reduction in grain size; increase in number of twins
2	5.5–10	350–950	Well developed shatter cones; pale yellow-white	4–7	85–95 (80–90)	0–10 (3–10)	None (none)	Trace (2–5)	5–15 (N/A)	Presence of "jigsaw" texture; fracturing of individual grains and generation of micro-breccias; symplectic regions along some (<15%) grain boundaries; PFs; PDFs	Calcite reduced to microbreccia
3a[e]	10–20	>1000	Difficult to discern individual grains	6–18	50–85 (45–80)	5–30 (0–20)	Trace (none)	(0–10) (18–32)	>30 (N/A)	Reduced grain size; multiple sets of PDFs; symplectic regions surrounding majority (>75%) of quartz grains;	Calcite reduced to microbreccia; calcite intermingled with SiO_2 glass between quartz grains
3b[e]	15–20	>1000	Difficult to discern individual grains	9–21	<30 (N/A)	30–90 (N/A)	5–10 (N/A)	(0–10) (N/A)	>30 (N/A)	Widespread development of diaplectic glass; vesicular SiO_2 glass in original pore spaces	Calcite melt intermingled with SiO_2 glass between quartz grains; infiltration of calcite into quartz grains; occurs as globules and euhedral crystals
4	20–30	>1000	Few recognizable grains; faint layering white	18–30	<30 (15–45)	20–60 (?)	10–30 (?)	0–10 (10–30)	10–20 (N/A)	Original texture of sandstone lost; major development of vesicular SiO_2 glass; symplectic regions surround all remaining quartz grains	Infiltration of calcite melt into quartz grains; calcite globules and euhedral crystals in SiO_2 glass
5a[e]	>30	>1000	Highly vesicular; white	30–36	<10 (0–15)	10–30 (?)	>70 (?)	Trace (0–5)	Trace (N/A)	Isolated remnant quartz grains; almost complete transformation to diaplectic or vesicular SiO_2 glass (lechatelierite)	Infiltration of calcite melt into quartz grains; calcite globules and euhedral crystals in SiO_2 glass
5b[e]	>30	>1000	Highly vesicular; white.	44–58	None (none)	<10 (none)	>90 (?)	Trace (0–5)	None (N/A)	Complete transformation to vesicular SiO_2 glass	Calcite melt globules and euhedral crystals in SiO_2 glass
6[f]	>30	>1000	Dense; gray; translucent	4–9	100 (N/A)	None (N/A)	None (N/A)	None (N/A)	None (N/A)	Recrystallized SiO_2 glass	Calcite melt globules and euhedral crystals in recrystallized quartz

[a]Pressures and post-shock temperatures from Kieffer et al. (1976).
[b]Average porosities for 5–10 samples per class were measured on representative digital BSE images using an image analysis program (Scion Image). The data presented represents the range of the measured average porosities.
[c]Values for Coconino Sandstone from Meteor Crater in parentheses for comparison (from Kieffer 1971). Abbreviations: Qtz = quartz; Dg = diaplectic quartz glass; Lech = lechatelierite or vesicular SiO_2 glass; Toast = toasted quartz; N/A = not applicable.
[d]XRD techniques indicate that calcite is the only $CaCO_3$ phase in the samples studied.
[e]Class subdivided in this study.
[f]New class in this study.

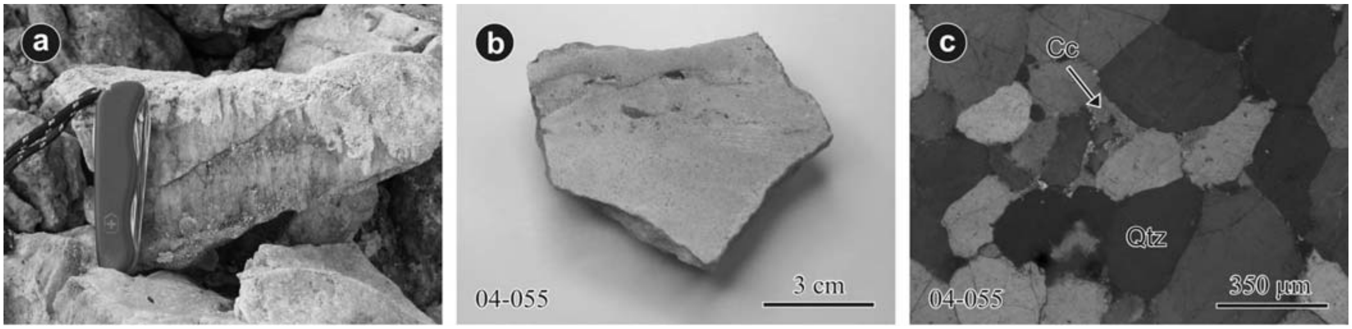

Fig. 3. Class 1 sandstones from the Haughton impact structure. a) Field photograph showing well-developed shatter cones in a megablock from the central part of the central uplift. The sandstones in this block are shocked to class 1b. 10 cm penknife for scale. b) Hand specimen image of a class 1b sandstone. c) Plane-polarized light photomicrograph of a class 1b sandstone. Note the presence of calcite (Cc) cement in places and the lack of porosity between quartz (Qtz) grains due to shock compression.

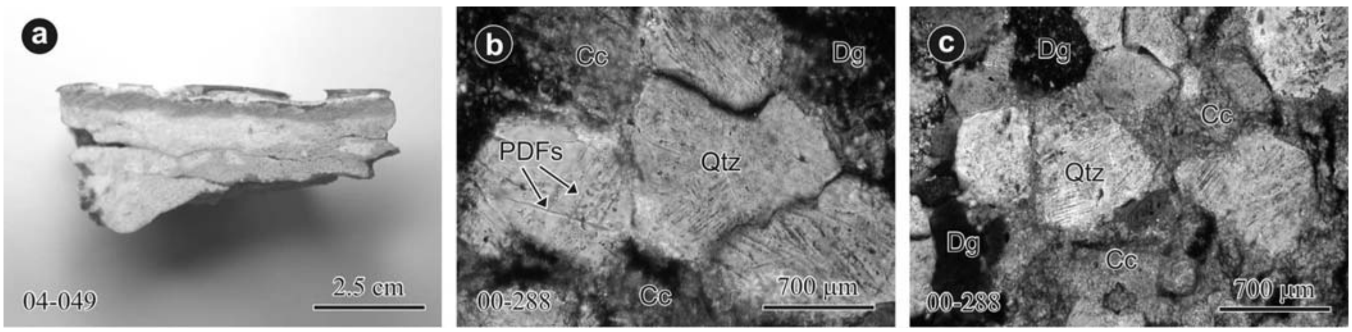

Fig. 4. Class 2 sandstones from the Haughton impact structure. a) Hand specimen image of a class 2 sandstone. b) and c) Plane-polarized light photomicrographs of a class 2 sandstones showing the well-developed "jigsaw" texture, first recognized in sandstones at Meteor Crater by Kieffer (1971). Shock metamorphic effects in quartz (Qtz) include the development of planar deformation features (PDFs) and diaplectic glass (Dg). Calcite (Cc) is reduced to a micro-breccia.

imagery, being characterized by their irregular mottled appearance (Figs. 5d, 5e). As with Coconino Sandstone from Meteor Crater (Kieffer et al. 1976b), nearly every quartz grain in class 3 samples at Haughton is rimmed by a thin symplectic region or opaque material (Figs. 5d, 5e). These symplectic regions also extend along fractures within quartz grains (Fig. 5d). Cryptocrystalline "cores" of coesite are present within many of these opaque regions (Fig. 5b); however, the opaque regions and the associated cores do not appear to be as abundant as the class 3 samples of Coconino Sandstone investigated by Kieffer et al. (1976b).

Class 3b sandstones are characterized by the widespread conversion of quartz into diaplectic glass (e.g., Figs. 5b, 5c where all quartz grains have been transformed into diaplectic glass). Sandstones from Haughton with coesite and diaplectic glass were previously recognized by Redeker and Stöffler (1988). K-feldspar has been observed in two class 3b samples, where it was partially or completely transformed into diaplectic glass. Class 3b sandstones are further characterized by the presence of small amounts of vesicular SiO_2-rich glass in the interstices between quartz grains (Figs. 5d, 5e). It is notable that two distinct phases of SiO_2-rich glass are present and observable in BSE images. The first type is pale gray in BSE images, identical to quartz, and yields high WDS totals (>99–101 wt%) and is pure SiO_2. WDS analyses indicate that the second darker glass is predominantly SiO_2, with less that 1 wt% other oxides, and displays consistently low totals (~85–92 wt%). This suggests the presence of substantial amounts of volatiles, likely H_2O, which is consistent with the dark appearance of this phase in BSE mode. This is consistent with experiments in the system SiO_2–H_2O, which demonstrate the existence of melts or supercritical fluids with the composition 75 wt% SiO_2, 25 wt% H_2O (Kennedy et al. 1962). Rapid quenching may, therefore, preserve H_2O-rich glasses.

Calcite in class 3 rocks is fundamentally different from that in class 1 and 2 samples (Table 2). X-ray microdiffraction and XRD analysis of powders indicate that no polymorphs of $CaCO_3$, such as aragonite, are present in any of the samples studied. It is notable that in class 3 samples, calcite is always coarser grained than in class 1b and 2 rocks, it lacks pervasive mechanical twins, and displays either euhedral crystal shapes or is present as globules embedded in SiO_2-rich glass (Figs. 5d, 5e). In one class 3b sandstone shown in Figs. 5f–i, calcite has infiltrated a shocked quartz grain. Importantly, a layer of SiO_2 glass occurs at the contact between remnant symplectic quartz and calcite. There are sharp and curved menisci between SiO_2 glass and calcite, and irregularly shaped

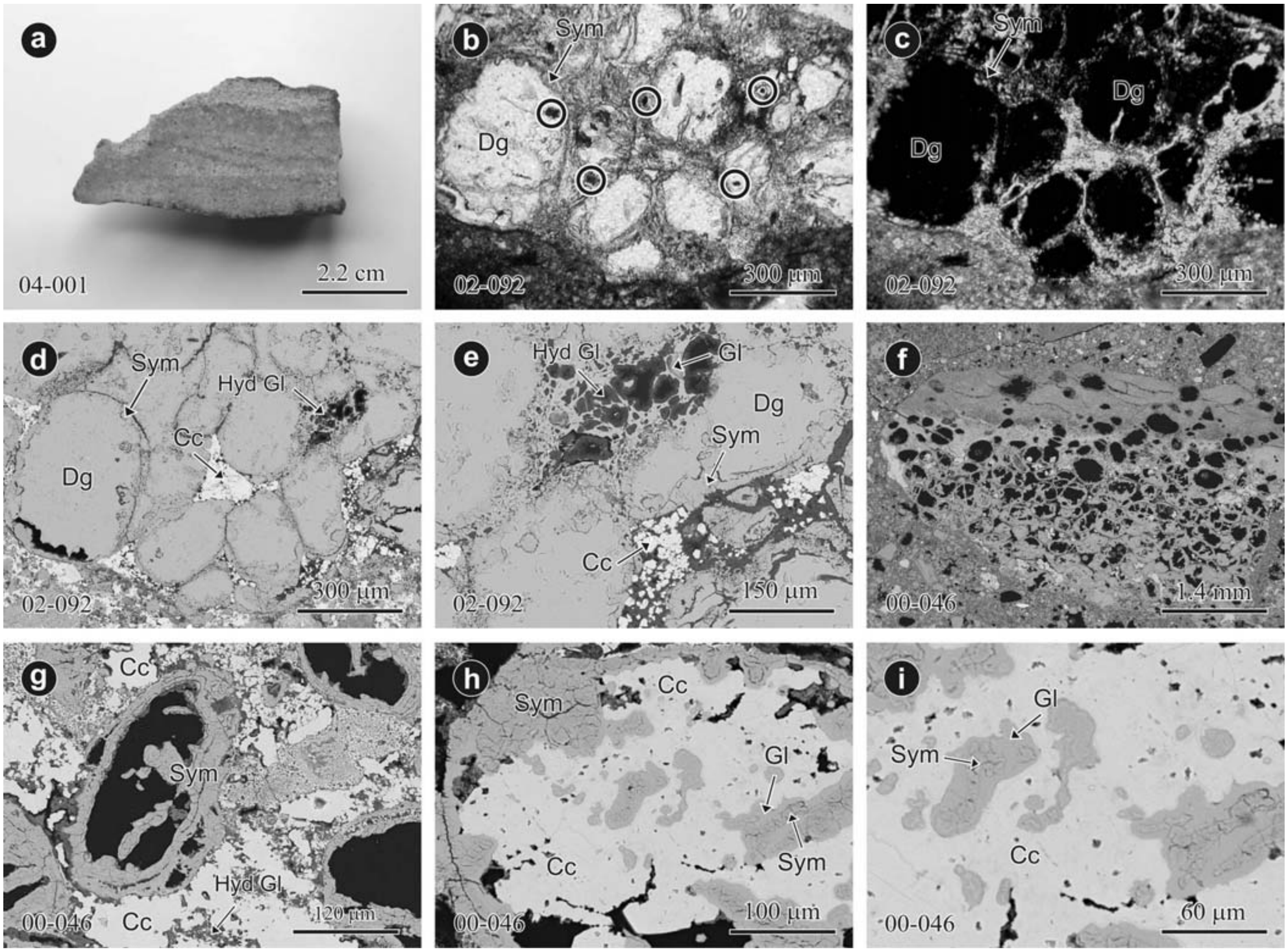

Fig. 5. Class 3 sandstones from the Haughton impact structure. a) Hand specimen image of a class 3 sandstone. b) and c) Plane- and cross-polarized light photomicrographs, respectively, of a class 3b sandstone in which quartz is almost completely transformed to diaplectic glass (Dg). The high relief "rims" of the quartz grains are symplectic intergrowths (Sym) of quartz, diaplectic glass, and coesite. The restriction of coesite to these "rims" has been confirmed by X-ray microdiffraction (see Fig. 6). The circles in Fig. 5b surround cryptocrystalline "cores" of coesite within opaque regions. d) Backscattered secondary electron image of the same region shown in Fig. 5b and c. Note the well-defined symplectic intergrowths (Sym) and the presence of calcite (Cc) and hydrous SiO_2-rich glass (Hyd Gl). e) Enlargement of a portion of Fig. 5d. Note the presence of two phases of SiO_2 glass within the original interstices between adjacent quartz grains. WDS analysis suggests that the dark SiO_2 glasses (Hyd Gl) contain up to ~12 wt% H_2O, whereas the brighter glass (Gl) is pure SiO_2. Irregularly shaped and euhedral calcite (Cc) grains are present in the SiO_2 glasses. f) Millimeter-size sandstone clast within crater-fill impact-melt breccias. g) Enlargement of a portion of Fig. 5f. Calcite (Cc) is intermingled with hydrous SiO_2 glass (Hyd Gl). Note the well-formed symplectic intergrowths (Sym) of quartz, diaplectic glass, and coesite. h) and i) Calcite (Cc) has infiltrated a shocked quartz grain, transformed to a symplectic intergrowth (Sym) of quartz, diaplectic glass, and coesite. Quartz is clearly melting in the calcite. Note the presence of a layer of SiO_2 glass (Gl) at the contact between the symplectic region and calcite. The textures indicate that calcite is an impact melt phase and is in the process of melting and assimilating the quartz, which requires post-shock temperatures of >1713 °C.

globules of SiO_2 glass with cores of symplectic quartz are present in the calcite.

Class 4 (~20 to 30 GPa)

Class 4 rocks are characterized by the almost complete loss of original sedimentary textures and grain relationships (Fig. 7a) except for a faint remnant lamination in a few samples (Table 2). Quartz is typically transformed to diaplectic glass with widespread development of symplectic intergrowths of quartz, coesite and diaplectic glass (Figs. 7b–d). Vesicular glass is more abundant than in class 3 rocks and is no longer confined to interstices between original quartz grains (Figs. 7d, 7e). K-feldspar in class 4 sandstones is completely transformed to vesicular glass (Fig. 7f). A notable feature of many class 4 samples is that the SiO_2 melt phases have recrystallized into microcrystalline quartz (e.g., Fig. 7d).

As with class 3 rocks, calcite in class 4 rocks is coarse-grained, lacks pervasive mechanical twins, and displays either euhedral crystal shapes or is present as globules within

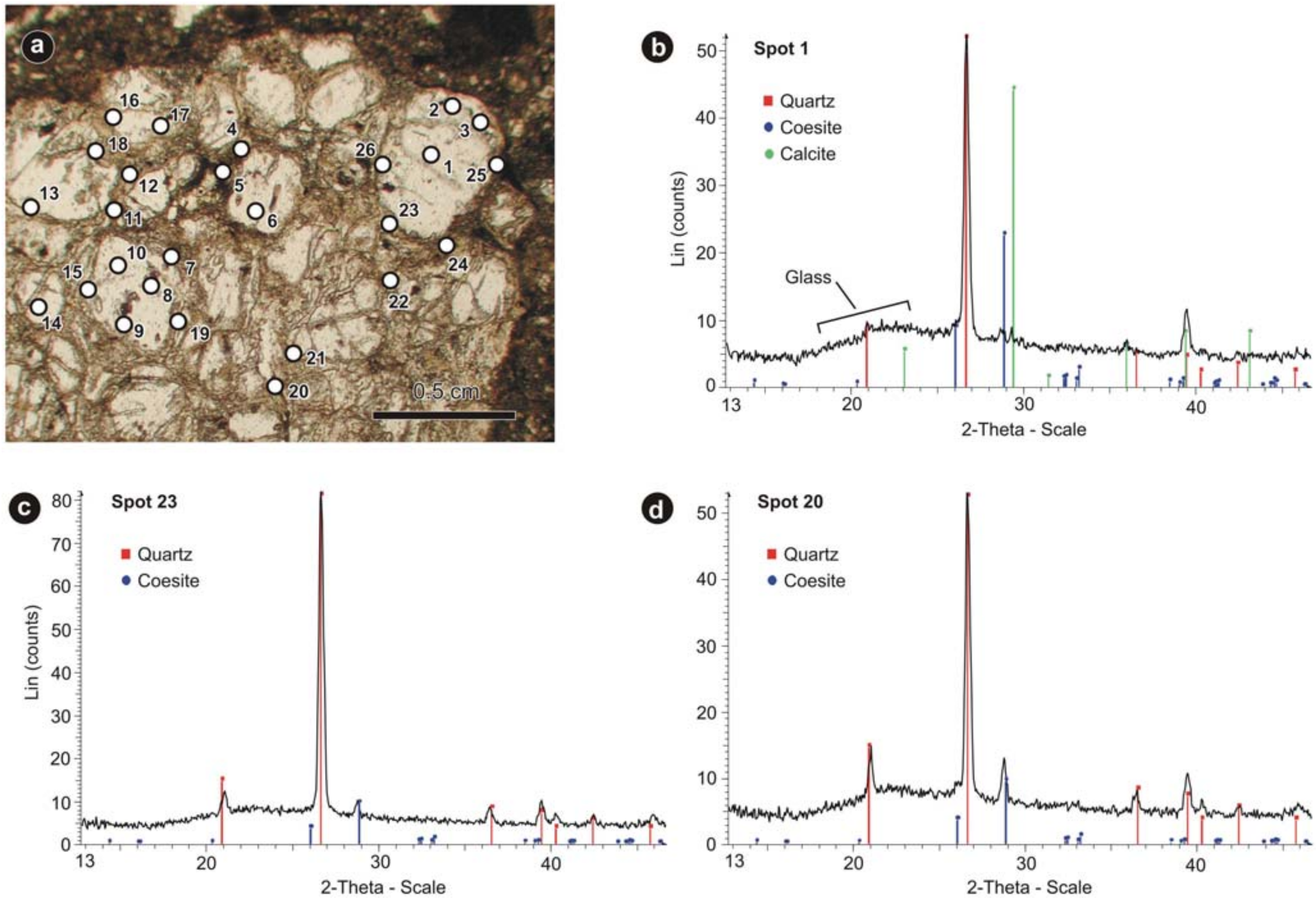

Fig. 6. X-ray microdiffraction results for a class 3 sandstone clast contained within crater-fill impact-melt breccias (same clast shown in Figs. 5b–e). a) Twenty-six single spot analyses were carried out. b) In cross-polarized light, this quartz grain appears to be completely transformed to diaplectic glass (Fig. 5c). X-ray microdiffraction analysis indicates that some quartz remains. Minor coesite and calcite is also present. Glass appears as a broad "hump" in the spectrum. c) and d) X-ray microdiffraction indicates that the high-relief rims of these quartz grains (see Fig. 6a) comprise quartz and coesite. Note the very prominent coesite peaks in (d).

K-feldspar and/or SiO_2-rich glass (Table 2). In several samples, calcite is intermingled with SiO_2-rich glass (e.g., Fig. 7e).

Class 5 (>30 GPa)

Class 5 sandstones at Haughton occur as low density (~0.6–1.4 gcm^{-3}) pumice-like clasts within the crater-fill impact melt breccias (Fig. 8a). These samples consist primarily of highly vesiculated SiO_2 glass or lechatelierite (Table 2) (Fig. 8). Class 5 rocks have been subdivided in this study based on the presence or absence of pre-impact protolith (Table 2): class 5a samples contain clasts or domains of shocked quartz and diaplectic quartz glass; whereas, class 5b rocks are comprised entirely of SiO_2 glass or lechatelierite. These SiO_2 glasses are typically intensely vesiculated, with vesicles, and delicate melt bridges on the micrometer scale, showing no sign of alteration (Figs. 8b–f). Flow textures are common (Figs. 8a, 8b, 8f). Class 5 glasses correspond to type C1 and C3 glasses of Osinski et al. (2005a). Calcite is present in class 5a and 5b samples, occurring as globules within SiO_2 glass (Figs. 8d, 8e). The calcite is unshocked and lacks mechanical twins.

Class 6 (>30 GPa)

This new class of impact-metamorphosed sandstone is characterized by a high density and a lack of clasts or vesicles (Table 2). In hand specimen, class 6 sandstones are opaque, cream to pale gray-colored and resemble 'flint' (Fig. 9a). Optical microscopy indicates that these samples are recrystallized to quartz (Figs. 9b, 9c). Class 6 sandstones include the type C3 glasses of Osinski et al. (2005a). Calcite occurs as globules and euhedral grains within class 6 sandstones (Figs. 9d–f). It is notable that class 6 samples glasses contain isolated spherical enclaves of hydrous SiO_2-rich glass (Fig. 9d; Osinski et al. 2005a). Importantly, these enclaves typically contain zoned, subhedral to euhedral crystals of calcite (Figs. 9d, 9e) that display unusual compositions (up to 8 wt% Al_2O_3 and 2 wt% SiO_2; Osinski et

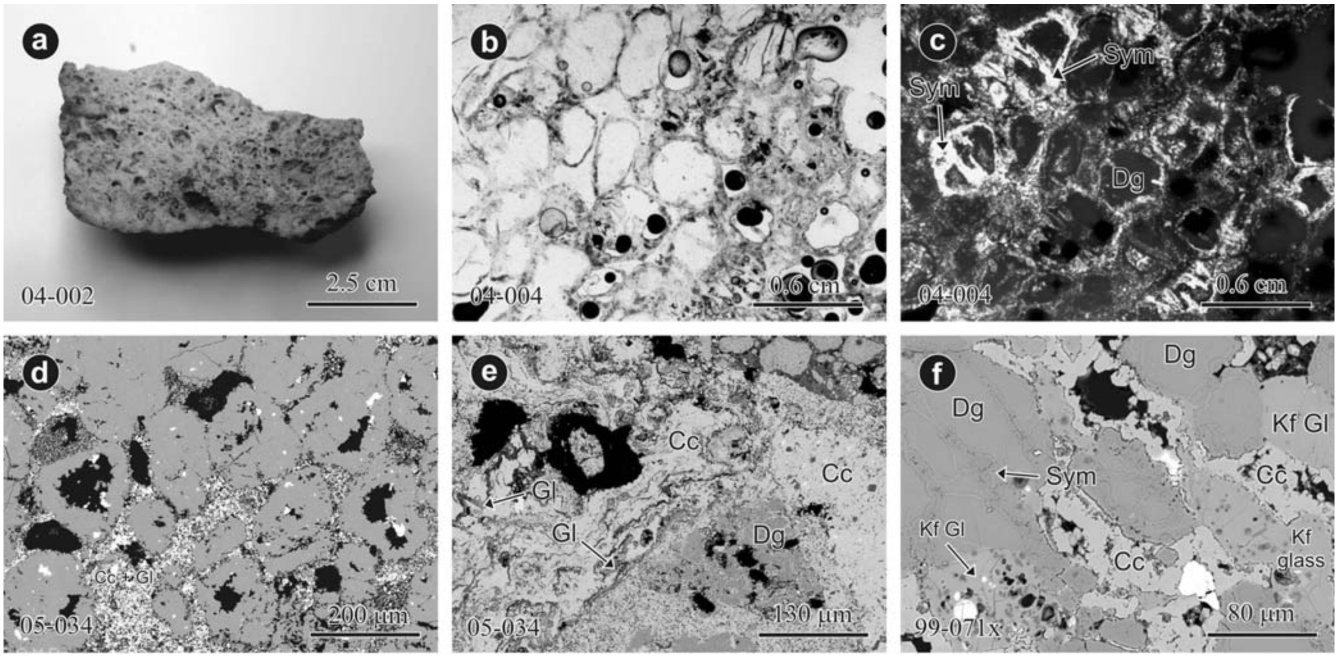

Fig. 7. Class 4 sandstones from the Haughton impact structure. a) Hand specimen image of a class 4 sandstone showing the complete loss of original sedimentary fabric. b) and c) Plane- and cross-polarized light photomicrographs, respectively, of a class 4 sandstone. Quartz has been transformed to diaplectic glass (Dg) and symplectic intergrowths (Sym) of quartz, diaplectic glass, and coesite. Note the destruction of original sedimentary fabrics such as layering. d) Backscattered secondary electron (BSE) image of recrystallized SiO_2 grains. Note the presence of calcite (Cc) intermingled with SiO_2 glass (Gl). e) BSE image showing flow textures developed between calcite (Cc) and SiO_2 glass (Gl) and a remnant grain of diaplectic glass (Dg). f) Class 4 sandstone in which K-feldspar is transformed to vesiculated glass (Kf Gl). Note the immiscible sphere of FeS_2 (bright) in the bottom left corner demonstrating the melting of sedimentary pyrite. Quartz has been completely transformed to diaplectic glass (Dg) and symplectic intergrowths (Sym) of quartz, diaplectic glass, and coesite. Calcite melt is intermingled with SiO_2 and K-feldspar glass (Kf Gl).

al. 2005a). It is not clear if the Si and Al is incorporated into the calcite structure or if Si and/or Al is present in nanometer-sized Ca–Al silicates that crystallized from the $CaCO_3$-rich melt during quenching (cf. Osinski et al. 2005a).

DISCUSSION AND CONCLUSIONS

Impact Metamorphism of Quartz in Sedimentary Targets

It is well known that the response of quartz to shock compression in porous sedimentary targets is fundamentally different from that in non-porous crystalline targets (Kieffer 1971; Kieffer et al. 1976b; Stöffler 1984; Grieve et al. 1996). This work has shown that the detailed classification scheme developed for sandstones from Meteor Crater is broadly applicable to Haughton and, therefore, likely for other terrestrial impact sites. The sandstones at Haughton can be classified into six different shock classes and display the same range of characteristic textures as seen at Meteor Crater (e.g., “jigsaw” textures and symplectic intergrowths of quartz, diaplectic glass, and coesite; Table 2).

As noted in the previous results section, the pressure and temperature estimates for the different shock classes used in this study are from Kieffer (1971) and Kieffer et al. (1976b). Those values were based on correlating shock effects in naturally shocked Coconino Sandstone from Meteor Crater, with observed effects in samples of the same lithology shocked to known pressures in laboratory experiments. It is known from these and other experiments (e.g., Housen and Holsapple 2003) and numerical modeling (e.g., Wünnemann and Collins 2007) that variation in porosity exerts considerable influence on the impact cratering process and the resultant shock effects. This must be considered when comparing the results of this study with those from Meteor Crater (Kieffer 1971; Kieffer et al. 1976b). Importantly, the average porosity of unshocked Coconino Sandstone (10 to 20%; Kieffer et al. 1976b) is similar to unshocked Haughton sandstones (5 to 25%). Thus, it is suggested that the pressure–temperature estimates for the various sandstone shock classes derived by Kieffer et al. (1976b) should be broadly applicable to Haughton. This view is supported by the major similarities between shock effects in quartz at Meteor Crater and Haughton (Table 2). The influence of calcite and other phases, such as K-feldspar, on the pressure–temperature history of shocked sandstones is difficult to determine without further shock experiments, which is beyond the scope of this study.

The major difference between the Haughton and Meteor Crater sandstones are in the moderately shocked samples. Diaplectic glass is more abundant at Haughton in class 3 and 4 rocks, whereas coesite is less well developed. This prompted

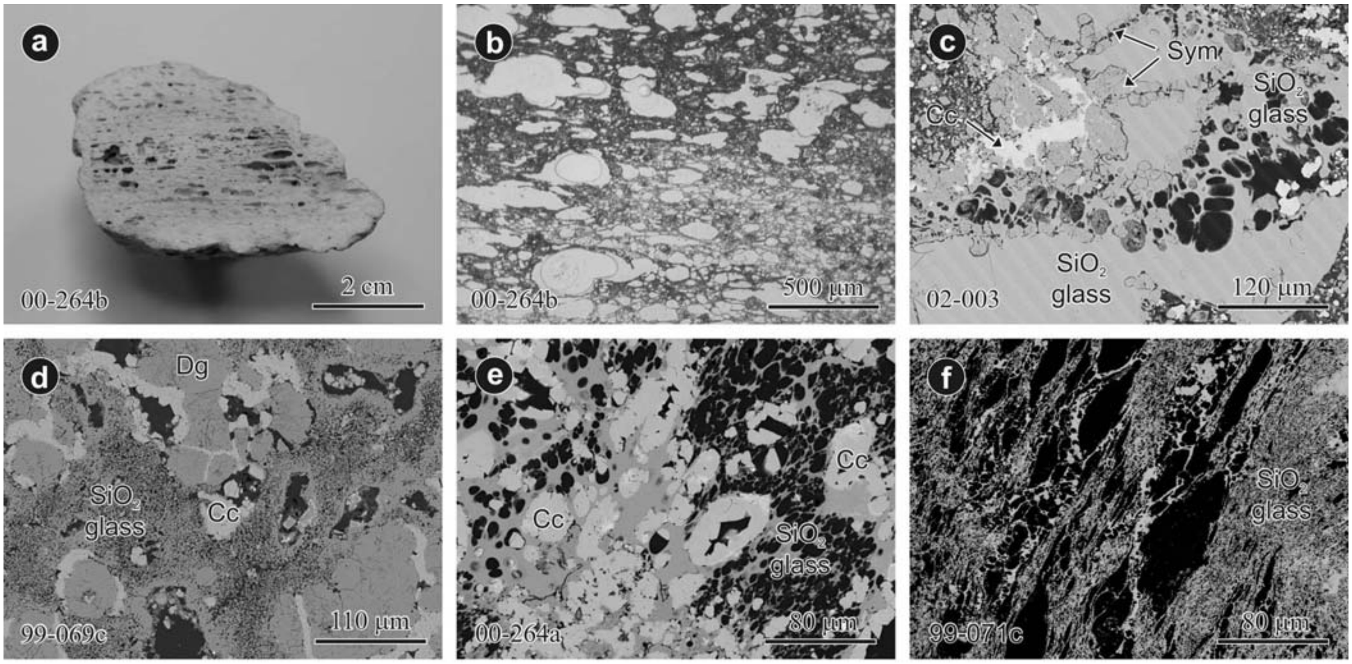

Fig. 8. Class 5 sandstones from the Haughton impact structure. (a) Hand specimen image of a highly vesiculated class 5b sandstone. (b) Plane-polarized light photomicrograph showing the intensely vesiculated nature of class 5b sandstones. (c) and (d) Backscattered secondary electron (BSE) images of class 5a sandstones. Note the presence of remnant diaplectic quartz glass (Dg) and symplectic intergrowths (Sym) of quartz, diaplectic glass, and coesite. Calcite (Cc) is intermingled with SiO_2 glass. (e) Globules of calcite (Cc) within vesiculated SiO_2 glass. (f) Flow-textured SiO_2 glass or lechatelierite in a class 5b sample.

the subclassification of class 3 samples in this study. The reason(s) for the enhanced development of diaplectic glass at Haughton are unclear, but could be due to a variety of factors including overall impact energy and volume of rocks affected by the shock wave (i.e., Haughton is substantially larger than Meteor Crater), and general differences in target properties, including the greater variety of pre-impact sandstone lithologies at Haughton compared to the relatively homogenous Coconino Sandstone at Meteor Crater. The heterogeneity of sandstone target rocks at Haughton may also be responsible for other minor differences in shock properties (Table 2). In particular, symplectic intergrowths of quartz, coesite and diaplectic glass and so-called opaque regions extend along fractures within quartz grains at Haughton, but not at Meteor Crater. Cryptocrystalline “cores” of coesite are also not as abundant at Haughton, compared to Meteor Crater where these features occur within 30 to 50% of the opaque regions (Kieffer et al. 1976b). It has been proposed that these cryptocrystalline “cores” of coesite are formed from jets of obliquely colliding grains shooting into collapsing pore spaces (Kieffer et al. 1976b). Thus, the formation of such cores will be influenced by differences in various properties, such as porosity, the abundance of pore water, and the proportion of other minerals (e.g., calcite, K-feldspar).

Toasted quartz is abundant in the shocked sandstones at Haughton. It is notable that toasted quartz has only been observed in samples of class 2 to 4. This correlates with the presence of PDFs, providing supporting evidence for the interpretation that toasted quartz results from the presence of microscopic fluid inclusions (Whitehead et al. 2002). These inclusions form as H_2O exsolves from the glass along the PDFs as it recrystallizes to quartz, forming so-called decorated PDFs.

An additional class of shocked sandstone has been added here to the original classification scheme of Kieffer (1971). Class 6 samples are typically dense, non-porous, opaque, and resemble flint or chert in hand specimen (Table 2). Optical microscopy and SEM studies show that these samples represent larger bodies of sandstone-derived melt that cooled slowly and recrystallized to microcrystalline quartz. This is in contrast to the highly vesiculated glassy class 5 rocks, which represent rapidly quenched sandstone-derived melts. Recrystallization of SiO_2 melt phases into quartz was also recognized in several class 4 samples, suggesting that post-impact thermal annealing and recrystallization of melt phases is an important process during mid- to large-size impact events. This was not recognized at Meteor Crater, consistent with its small size and small volume of impact melt (Kieffer 1971).

It is interesting to note that ballen quartz is absent at Haughton. The formation of the “ballen” structure has been attributed to the volume change resulting from the inversion of β- to α-cristobalite, which in turn formed from SiO_2 glass or lechatelierite (Carstens 1975). This implies pressures >50 to 55 GPa. Alternatively, ballen quartz may represent recrystallized/devitrified diaplectic quartz glass, which implies pressures of >30 to <55 GPa (Bischoff and Stöffler 1984), as well as recrystallized lechatelierite. Both these interpretations

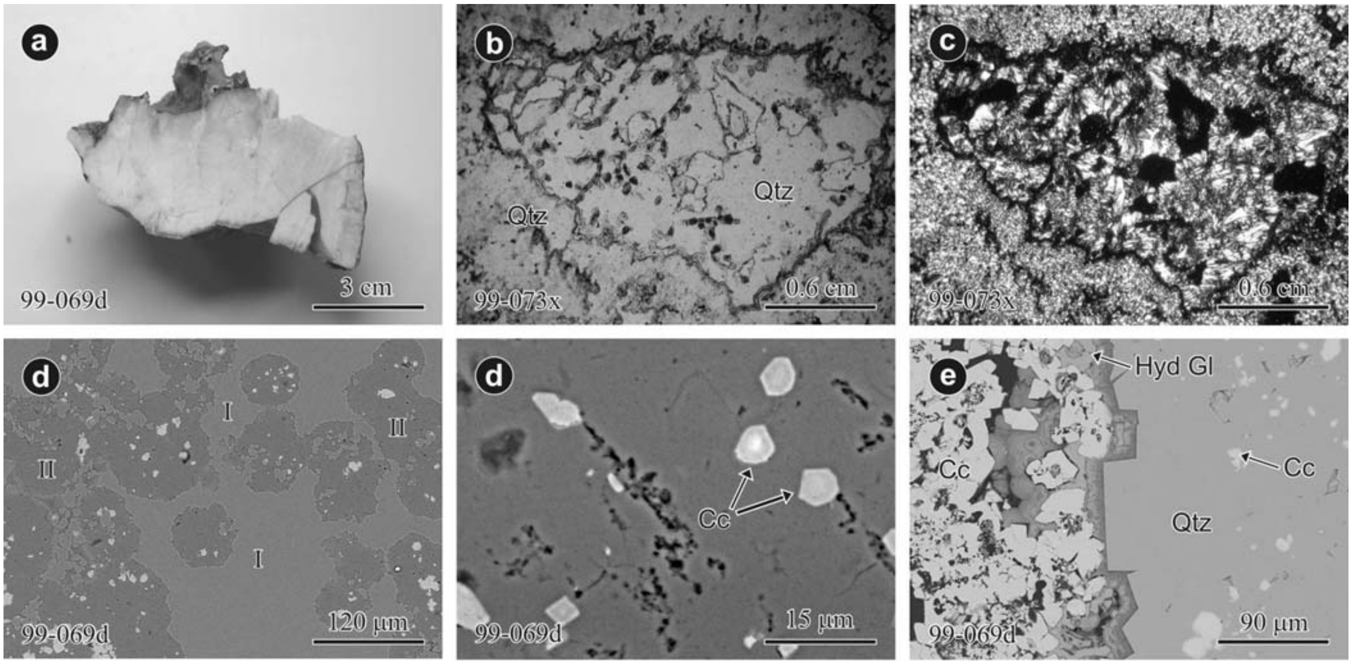

Fig. 9. Class 6 sandstones from the Haughton impact structure. a) Hand specimen image of a class 6 sandstone. Note the lack of vesicles. b) and c) Plane- and cross-polarized light photomicrographs, respectively, of a class 6 sandstone, showing the almost complete recrystallization of originally glassy SiO_2 phase to quartz (Qtz). d) and e) Two distinct SiO_2 glass phases within a class 6 sample. The first variety (I) consists of large, originally glassy, spherules that have recrystallized to quartz, enclosing smaller, coalesced globular masses of glass (II). The glasses are H_2O-rich (~8–10 wt%) and contain abundant microscopic subhedral to euhedral calcite (Cc) crystals, which contain up to ~8 wt% Al_2O_3 and ~2 wt% SiO_2 (Osinski et al. 2005). f) Globules of calcite (Cc) within recrystallized SiO_2 glass (Qtz) (right of image) next to a region of euhedral calcite crystals and hydrous SiO_2 glass (Hyd Gl) (left of image).

have been questioned based on the observation of ballen quartz displaying PDFs at the Deep Bay impact structure, Canada (Smith et al. 1999); however, this work has yet to be confirmed and is only available in abstract form. Importantly, SiO_2 glasses are abundant at Haughton, so why is ballen quartz absent?

It is notable that ballen quartz has only been documented in impactites at impact structures developed in crystalline target rocks (Carstens 1975; Grieve 1975; Bischoff and Stöffler 1984; Schuraytz and Dressler 1997; Smith et al. 1999). Ballen quartz is present at the Ries impact structure, Germany (Engelhardt 1972), which formed in a mixed crystalline-sedimentary target sequence; however, it is clear that ballen quartz only occurs in coherent impact melt rocks at the Ries structure, which are derived from the crystalline basement (Osinski 2004). Ballen quartz is not present in the suevite deposits (Osinski et al. 2004), which are derived from a combination of sedimentary and crystalline target rocks. These observations together with its absence at Haughton, suggests that ballen quartz does not form in impactites derived from sedimentary rocks. In terms of potential formation mechanisms, if ballen quartz does indeed form from recrystallized and/or devitrified SiO_2 glasses (Carstens 1975; Bischoff and Stöffler 1984), cooling rate may be an important constraint: sediment-derived impact melts are typically rapidly quenched compared to melts generated from crystalline targets (Osinski et al. 2005a). However, the exact formation mechanism of ballen quartz remains elusive and further work is required. In particular, the preliminary observations of Smith et al. (1999) from the Deep Bay structure need to be confirmed or disproved.

A characteristic of class 3 and 4 sandstones at Haughton is the presence of hydrous (i.e., H_2O-rich) glasses as globules within SiO_2 glass or forming isolated 'pockets' between shocked quartz grains (e.g., Figs. 5d, 5e). Kieffer et al. (1976b) showed that in highly shocked sandstones from Meteor Crater, H_2O and SiO_2 intermixed to form a supercritical fluid during shock compression; H_2O exsolves out of this fluid during the subsequent rarefaction event. A simple explanation for the hydrous glasses in the Haughton samples is, therefore, that they represent quenched supercritical fluids or hydrous impact melts. Hydrous melts and solute-rich supercritical fluids containing >40–50 wt% H_2O are not uncommon in endogenic igneous systems (Bureau and Keppler 1999; Clifford 1999). H_2O-rich glasses have also been documented at other impact sites (Osinski 2003; Harris and Schultz 2005), suggesting that this is an important phenomenon during hypervelocity impact events and that not all impact-generated glasses are volatile-poor.

Impact Metamorphism of Calcite

Carbonates form an important component of the target sequence of approximately one third of the world's known impact structures (Earth Impact Database 2007). Recent investigations of terrestrial impact structures (Graup 1999;

Jones et al. 2000; Osinski and Spray 2001; Osinski et al. 2005a; Pratesi et al. 2005) and improvements to the phase diagram of $CaCO_3$ (Ivanov and Deutsch 2002) have shown that impact melting is important during hypervelocity impact into carbonates (see Osinski et al. 2008 for a review). However, the exact pressure-temperature conditions under which melting occurs are not known.

This work enables a comparison, for the first time, between the impact metamorphic effects of calcite with known, calibrated effects in quartz. No indications of shock were found in calcite in class 1a sandstones. In class 1b and 2 sandstones from Haughton, calcite displays an increase in the abundance of mechanical twins and is typically reduced to fine-grained polycrystalline "microbreccias." This is consistent with previous studies of shocked limestones, which showed that plastic deformation of calcite is minor; rather, deformation appears to produce pulverization and consolidation (Barber and Wenk 1973). No evidence for melting or decomposition is seen in class 1 and 2 rocks at Haughton.

In samples classified as class 3a and higher, calcite lacks a high density of mechanical twins and is not brecciated. Instead, it appears fresh, unshocked, and is present as rounded micro-crystalline globules and/or euhedral crystals within SiO_2 and K-feldspar glasses (Table 2). These silicate glasses represent quenched impact melt derived from quartz and K-feldspar. The textural relationships documented in this study clearly show that calcite in class 3a and higher sandstones, has also undergone melting. This is consistent with previous studies at Haughton, which demonstrated the impact melt origin of calcite in the groundmass of the crater-fill impact melt breccias (Osinski and Spray 2001; Osinski et al. 2005a). The same textural and geochemical indicators of melting documented in these earlier studies are also present in the impact-metamorphosed sandstones studied here. In particular, the intermingling, but not mixing, of silicate glasses and calcite (e.g., Figs. 5h, 5i), the curved menisci with sharp boundaries between these phases (e.g., Figs. 5h, 5i; 7d, 7e), and the presence of flow textures (e.g., Fig. 7e), provides clear evidence for the melting of calcite. This is supported by the lack of any alteration of SiO_2-rich glasses associated with carbonates, which rules out a hydrothermal origin for the calcite.

Importantly, the textural evidence presented here, when combined with the quantitative data of Kieffer (1971) and Kieffer et al. (1976b), constrains the onset of melting of calcite in the Haughton sandstones to >10<20 GPa (i.e., in class 3 rocks and above), corresponding to post-shock temperatures of >1250 K (Kieffer 1971). When compared to the phase relations of $CaCO_3$—which suggest that the conditions required for calcite to melt are >1 GPa at post-shock temperatures in excess of 1500 K (Ivanov and Deutsch 2002)—it is apparent that temperature is the limiting factor and explains why melting of calcite did not occur in the Haughton sandstones at pressures <10 GPa (i.e., the corresponding shock temperatures were not high enough). As such, factors such as porosity will be extremely important in determining the conditions under which calcite melts during hypervelocity impact. For example, the dramatically lower pressure–temperature conditions under which quartz melts in porous and non-porous targets (Fig. 1) may also be the case for calcite so that in low-porosity limestones, the pressures required for the onset of whole rock melting may be significantly higher than in the porous calcite-bearing sandstones studied here.

It is notable that no evidence for the decomposition of calcite during the Haughton impact event was found in this current study (cf. Osinski et al. 2005a). This is consistent with the phase relations of $CaCO_3$, which suggest that decomposition can only occur after pressure release due to high residual temperatures during post-shock cooling (>1200 K; Ivanov and Deutsch 2002). As noted in a recent review, the decomposition of calcite appears to be a post-impact contact metamorphic process (Osinski et al. 2008), restricted to high-temperature silicate melt-rich impactites (e.g., impact melt-bearing breccias at the Ries [Baranyi 1980] and Chicxulub [Deutsch et al. 2003] impact structures). At Haughton, it is clear that the sediment-derived impact melts were rapidly quenched (Osinski et al. 2005a), so that decomposition was likely limited.

Acknowledgments–Many of the samples investigated for this study were collected while the author was a graduate student at the University of New Brunswick, Fredericton, Canada, and for this, sincere thanks go to John Spray. Lang Shi of the Microanalysis Laboratory at McGill University provided valuable help during electron microprobe studies. Roberta L. Flemming and Matthew Izawa are thanked for carrying out the X-ray microdiffraction analyses. The author was supported by the Canadian Space Agency (CSA) and the Natural Sciences and Engineering Research Council of Canada (NSERC), through the Visiting Fellowships in Canadian Government Laboratories program. A. Deutsch, S. W. Kieffer, and an anonymous colleague are thanked for their detailed and constructive reviews.

Editorial Handling—Dr. Alexander Deutsch

REFERENCES

Agrinier P., Deutsch A., Schärer U., and Martinez I. 2001. Fast back-reactions of shock-released CO_2 from carbonates: An experimental approach. *Geochimica et Cosmochimica Acta* 65: 2615–2632.

Badjukov D. D., Dikov Y. P., Petrova T. L., and Pershin S. V. 1995. Shock behavior of calcite, anhydrite, and gypsum (abstract). 26th Lunar and Planetary Science Conference. pp. 63–64.

Baranyi I. 1980. Untersuchungen über die Veränderungen von Sedimentgesteinseinschlüssen im Suevit des Nördlinger Rieses. *Beiträge zur Naturkundlichen Forschung Südwest-Deutschlands* 39:37–56.

Barber D. J. and Wenk H. R. 1973. The microstructure of

experimentally deformed limestones. *Journal of Materials Science* 8:500–508.
Bell M. S. 2001. Thermal gravimetric analysis of experimentally shocked calcite (abstract). *Meteoritics & Planetary Science* 36: A17.
Bell M. S., Hörz F., and Reid A. 1998. Characterization of experimental shock effects in calcite and dolomite by X-ray diffraction (abstract #1422). 29th Lunar and Planetary Science Conference. CD-ROM.
Bischoff A. and Stöffler D. 1984. Chemical and structural changes induced by thermal annealing of shocked feldspar inclusions in impact melt rocks from Lappajärvi crater, Finland. *Journal of Geophysical Research* 89:B645–B656.
Boslough M. B., Ahrens T. J., Vizgirda J., Becker R. H., and Epstein S. 1982. Shock-induced devolatilization of calcite. *Earth and Planetary Science Letters* 61:166–170.
Bureau H. and Keppler H. 1999. Complete miscibility between silicate melts and hydrous fluids in the upper mantle: Experimental evidence and geochemical implications. *Earth and Planetary Science Letters* 165:187–196.
Burt J. B., Pope K. O., and Watkinson A. J. 2005. Petrographic, X-ray diffraction and electron spin resonance analysis of deformed calcite: Meteor Crater, Arizona. *Meteoritics & Planetary Science* 40:296–305.
Carstens H. 1975. Thermal history of impact melt rocks in the Fennoscandian Shield. *Contributions to Mineralogy and Petrology* 50:145–155.
Clifford T. 1999. *Fundamentals of supercritical fluids*. New York: Oxford University Press. pp. 228.
Deutsch A., Langenhorst F., Hornemann U., and Ivanov B. A. 2003. On the shock behavior of anhydrite and carbonates—Is post-shock melting the most important effect? Examples from Chicxulub (abstract #4080). 3rd International Conference on Large Meteorite Impacts. CD-ROM.
Earth Impact Database. 2007. http://www.unb.ca/passc/Impact Database. Accessed: 15 April 2007.
Engelhardt W. V. 1972. Shock-produced rock glasses from the Ries crater. *Contributions to Mineralogy and Petrology* 36:265–292.
French B. M. and Short N. M., eds. 1968. *Shock metamorphism of natural materials*. Baltimore: Mono Book Corp. 644 p.
Graup G. 1999. Carbonate-silicate liquid immiscibility upon impact melting: Ries crater, Germany. *Meteoritics & Planetary Science* 34:425–438.
Grieve R. A. F. 1975. Petrology and chemistry of impact melt at Mistastin Lake crater, Labrador. *Geological Society of America Bulletin* 86:1617–1629.
Grieve R. A. F. 1988. The Haughton impact structure: Summary and synthesis of the results of the HISS Project. *Meteoritics* 23:249–254.
Grieve R. A. F., Langenhorst F., and Stöffler D. 1996. Shock metamorphism of quartz in nature and experiment: II. Significance in geoscience. *Meteoritics & Planetary Science* 31: 6–35.
Harris R. S. and Schultz P. H. 2005. The significance of hydrous glasses in Argentine impact melt breccias (abstract #5267). 68th Annual Meeting of the Meteoritical Society. CD-ROM.
Housen K. R. and Holsapple K. A. 2003. Impact cratering on porous asteroids. *Icarus* 163:102–119.
Ivanov B. A. and Deutsch A. 2002. The phase diagram of $CaCO_3$ in relation to shock compression and decompression. *Physics of the Earth and Planetary Interiors* 129:131–143.
Ivanov B. A., Langenhorst F., Deutsch A., and Hornemann U. 2002. How strong was impact-induced CO_2 degassing in the K/T event? Numerical modeling of laboratory experiments. In *Catastrophic events and mass extinctions: Impacts and beyond*, edited by Koeberl C. and MacLeod K. G. GSA Special Paper #356. Boulder, Colorado: Geological Society of America. pp. 587–594.
Jones A. P., Claeys P.; and Heuschkel S. 2000., Impact melting of carbonates from the Chicxulub crater. In *Impacts and the early Earth*, edited by Gilmour I. and Koeberl C. Lecture Notes in Earth Sciences, vol. 91. Berlin: Springer-Verlag. pp. 343–361.
Kennedy G. C., Wasserburg G. J., Heard H. C., and Newton R. C. 1962. The upper three-phase region in the system SiO_2–H_2O. *American Journal of Science* 260:501–521.
Kieffer S. W. 1971. Shock metamorphism of the Coconino Sandstone at Meteor Crater, Arizona. *Journal of Geophysical Research* 76: 5449–5473.
Kieffer S. W. and Simonds C. H. 1980. The role of volatiles and lithology in the impact cratering process. *Reviews of Geophysics and Space Physics* 18:143–181.
Kieffer S. W., Schaal R. B., Gibbons R., Hörz F., Milton D. J.; and Dube A. 1976a. Shocked basalt from Lonar impact crater, India, and experimental analogues. Proceedings, 7th Lunar Science Conference. pp. 1391–1412.
Kieffer S. W., Phakey P. P., and Christie J. M. 1976b. Shock processes in porous quartzite: Transmission electron microscope observations and theory. *Contributions to Mineralogy and Petrology* 59:41–93.
Kondo K. I. and Ahrens T. J. 1983. Heterogeneous shock-induced thermal radiation in minerals. *Physics and Chemistry of Minerals* 9:173–181.
Kotra R. K., See J. H., Gibson E. K. J., Hörz F., Cintala M. J., and Schmidt R. M. 1983. Carbon dioxide loss in experimentally shocked calcite and limestone (abstract). 14th Lunar and Planetary Science Conference. pp. 401–402.
Lange M. A. and Ahrens T. J. 1986. Shock-induced CO_2 loss from $CaCO_3$; implications for early planetary atmospheres. *Earth and Planetary Science Letters* 77:409–418.
Langenhorst F., Deutsch A., Ivanov B. A., and Hornemann U. 2000. On the shock behavior of $CaCO_3$: Dynamic loading and fast unloading experiments-modeling-mineralogical observations (abstract #1851). 31st Lunar and Planetary Science Conference. CD-ROM.
Langenhorst F., Boustie M., Deutsch A., Hornemann U., Matignon Ch., Migault A., and Romain J. P. 2002. Experimental techniques for the simulation of shock metamorphism: A case study on calcite. In *High-pressure shock compression of solids V: Shock chemistry and meteoritic applications*, edited by Davison L., Horie Y., and Sekine T. Berlin–Heidelberg–New York: Springer. pp. 1–27. In *Large meteorite impacts and planetary evolution II*, edited by Dressler B. O. and Sharpton V. L. GSA Special Paper #339. Boulder, Colorado: Geological Society of America. pp. 205–214.
Martinez I., Agrinier P., Schärer U., and Javoy M. 1994a. A SEM–ATEM and stable isotope study of carbonates from the Haughton impact crater, Canada. *Earth and Planetary Science Letters* 121: 559–574.
Martinez I., Schärer U., Guyot F., Deutsch A. and Hornemann U. 1994b. Experimental and theoretical investigation of shock induced outgassing of dolomite (abstract). 25th Lunar and Planetary Science Conference. pp. 839.
Martinez I., Deutsch A., Schärer U., Ildefonse P., Guyot F. and Agrinier P. 1995. Shock recovery experiments on dolomite and thermodynamical calculations of impact induced decarbonation. *Journal of Geophysical Research* 100:15,465–15,476.
Metzler A., Ostertag R., Redeker H. J., and Stöffler D. 1988. Composition of the crystalline basement and shock metamorphism of crystalline and sedimentary target rocks at the Haughton impact crater, Devon Island, Canada. *Meteoritics* 23: 197–207.
Osinski G. R. 2003. Impact glasses in fallout suevites from the Ries

impact structure, Germany: An analytical SEM study. *Meteoritics & Planetary Science* 38:1641–1668.

Osinski G. R. 2004. Impact melt rocks from the Ries impact structure, Germany: An origin as impact melt flows? *Earth and Planetary Science Letters* 226:529–543.

Osinski G. R. 2005. Shock-metamorphosed and shock-melted $CaCO_3$-bearing sandstones from the Haughton impact structure, Canada: Melting of calcite at ~10–20 GPa (abstract #2038). 36th Lunar and Planetary Science Conference. CD-ROM.

Osinski G. R. and Spray J. G. 2001. Impact-generated carbonate melts: Evidence from the Haughton structure, Canada. *Earth and Planetary Science Letters* 194:17–29.

Osinski G. R. and Spray J. G. 2003. Evidence for the shock melting of sulfates from the Haughton impact structure, Arctic Canada. *Earth and Planetary Science Letters* 215:357–370.

Osinski G. R. and Spray J. G. 2005. Tectonics of complex crater formation as revealed by the Haughton impact structure, Devon Island, Canadian High Arctic. *Meteoritics & Planetary Science* 40:1813–1834.

Osinski G. R., Grieve R. A. F., and Spray J. G. 2004. The nature of the groundmass of surficial suevites from the Ries impact structure, Germany, and constraints on its origin. *Meteoritics & Planetary Science* 39:1655–1684.

Osinski G. R., Spray J. G., and Lee P. 2005a. Impactites of the Haughton impact structure, Devon Island, Canadian High Arctic. *Meteoritics & Planetary Science* 40:12:1789–1812.

Osinski G. R., Lee P., Spray J. G., Parnell J., Lim D., Bunch T. E., Cockell C. S., and Glass B. 2005b. Geological overview and cratering model of the Haughton impact structure, Devon Island, Canadian High Arctic. *Meteoritics & Planetary Science* 40: 1759–1776.

Osinski G. R., Spray J. G. and Grieve R. A. F. 2008. Impact melting in sedimentary target rocks: An assessment. In *The sedimentary record of meteorite impacts*, edited by Evans K. R., Horton W., King D. K. Jr., Morrow J. R., and Warme J. E. GSA Special Paper #437. Boulder, Colorado: Geological Society of America. doi: 10.1130/2008.2437(01).

Polanskey C. A. and Ahrens T. J. 1994. Scaling craters in carbonates: Electron paramagnetic resonance analysis of shock damage. *Journal of Geophysical Research* 99:5621–5638.

Pratesi G., Morelli M., Rossi A. P., and Ori G. G. 2005. Chemical compositions of impact-melt breccias and target rocks from the Tenoumer impact crater, Mauritania. *Meteoritics & Planetary Science* 40:1653–1672.

Redeker H. J. and Stöffler D. 1988. The allochthonous polymict breccia layer of the Haughton impact crater, Devon Island, Canada. *Meteoritics* 23:185–196.

Robertson P. B. and Mason G. D. 1975. Shatter cones from Haughton Dome, Devon Island, Canada. *Nature* 255:393.

Robertson P. B. and Grieve R. A. F. 1978. The Haughton impact structure. *Meteoritics* 13:4:615–618.

Schedl A. 2006. Applications of twin analysis to studying meteorite impact structures. *Earth and Planetary Science Letters* 244:530–540.

Schuraytz B. C. and Dressler B. O. 1997. Ballen-structured quartz in glasses of the Wanapitei impact structure, Ontario, Canada (abstract #1773). 28th Lunar and Planetary Science Conference. CD-ROM.

Skála R. and Jakeš P. 1999. Shock-induced effects in natural calcite-rich targets as revealed by X-ray powder diffraction. In *Large meteorite impacts and planetary evolution II*, edited by B. O. Dressler and V. L. Sharpton. GSA Special Paper #339. Boulder, Colorado: Geological Society of America. pp. 205–214.

Skála R., Hörz F., and Jakes P. 1999. X-ray powder diffraction study of experimentally shocked dolomite (abstract 1327). 30th Lunar and Planetary Science Conference. CD-ROM.

Skála R., Ederová J., Matìjka P. and Hörz F. 2002. Mineralogical investigation of experimentally shocked dolomite: Implications for the outgassing of carbonates. In *Catastrophic events and mass extinctions: Impacts and beyond*, edited by Koeberl C. and MacLeod K. G. GSA Special Paper #356. Boulder, Colorado: Geological Society of America. pp. 571–586.

Smith J. J., Therriault A. M., and Pan Y. 1999. Ballen quartz from the Deep Bay impact structure (abstract). *Meteoritics & Planetary Science* 34:A110–A111.

Stöffler D. 1971. Progressive metamorphism and classification of shocked and brecciated crystalline rocks at impact craters. *Journal of Geophysical Research* 76:5541–5551.

Stöffler D. 1984. Glasses formed by hypervelocity impact. *Journal of Non-Crystalline Solids* 67:465–502.

Stöffler D. and Grieve R. A. F. 1994. Classification and nomenclature of impact metamorphic rocks: A proposal to the IUGS Subcommission on the Systematics of Metamorphic Rocks (abstract #1347). 25th Lunar and Planetary Science Conference. CD-ROM.

Thorsteinsson R. and Mayr U. 1987. *The sedimentary rocks of Devon Island, Canadian Arctic Archipelago, Geological Survey of Canada Memoir 411*. Ottawa: Geological Survey of Canada. pp. 182.

Tyburczy J. A. and Ahrens T. J. 1986. Dynamic compression and volatile release of carbonates. *Journal of Geophysical Research* 91:4730–4744.

Vizgirda J. and Ahrens T. J. 1982. Shock compression of aragonite and implications for the equation of state for carbonates. *Journal of Geophysical Research* 87:4747–4758.

Whitehead J., Spray J. G. and Grieve R. A. F. 2002. Origin of "toasted" quartz in terrestrial impact structures. *Geology* 30:431–434.

Wünnemann K. and Collins G. S. 2007. The effect of porosity on impact melt production (abstract #1514). 38th Lunar and Planetary Science Conference. CD-ROM.

APPENDIX

Table A1. Sampling locations for samples investigated in detail as part of this work.

Sample no.	UTM position[a] Easting	Northing
99-008	428,320	8,366,905
99-051	425,760	8,367,315
99-067c	424,690	8,368,155
99-069a	424,610	8,368,115
99-069c	424,610	8,368,115
99-069d	424,610	8,368,115
99-071a	424,560	8,367,865
99-071b	424,560	8,367,865
99-071c	424,560	8,367,865
99-071c	424,560	8,367,865
99-073x	425,550	8,369,965
99-074	424,890	8,372,905
99-075	424,770	8,372,835
99-087b	429,040	8,372,665
99-095	428,370	8,369,995
99-114a	424,410	8,368,665
99-114b	424,410	8,368,665
99-114c	424,410	8,368,665
00-174b	418,560	8,363,375
00-263a	425,570	8,367,675
00-263b	425,570	8,367,675
00-264a	425,570	8,367,675

Table A1. *Continued.* Sampling locations for samples investigated in detail as part of this work.

Sample no.	UTM position[a] Easting	Northing
00-264b	425,570	8,367,675
00-266	424,860	8,368,245
00-267	424,860	8,368,245
00-284	425,110	8,370,305
02-107	427,470	8,370,565
02-142	425,420	8,366,155
04-001	418,585	8,364,468
04-002	418,585	8,364,468
04-003	418,585	8,364,468
04-004	418,585	8,364,468
04-005	418,585	8,364,468
04-049	426,693	8,370,367
04-052	425,971	8,371,726
04-055	424,413	8,368,782
04-056	424,413	8,368,782
05-034	418,614	8,364,225
06-066	424,774	8,368,499
06-067	424,774	8,368,499
06-068	424,774	8,368,499
06-069	424,774	8,368,499
06-070	424,774	8,368,499

[a]UTM Zone 15N, NAD83 datum.